Half-Cone Beam Collimation for Triple-Camera SPECT Systems

Jianying Li, Ronald J. Jaszczak, Arnold Van Mullekom, Christopher Scarfone, Kim L. Greer and R. Edward Coleman
Department of Radiology, Duke University Medical Center, Durham, North Carolina; Department of Physics, North Carolina State University, Raleigh, North Carolina; and Nuclear Fields, St. Mary's, Australia

Cone-beam collimators provide increased sensitivity at similar resolution compared to other collimators. The use of cone-beam collimators for brain imaging with triple-camera SPECT systems, however, results in truncation of the base of the brain because of clearance of the shoulders. A half-cone beam collimator does not have the problem of truncation. The objective of this study was to compare the performance characteristics of half-cone beam with parallel-beam and fan-beam collimators with similar resolution characteristics for SPECT imaging of the brain. **Methods:** A half-cone beam collimator with the focal point located towards the base of the brain was built for a triple-camera SPECT system. Spatial resolutions and sensitivities of three collimators were measured. **Results:** When 10-cm from the collimator surface, the planar spatial resolutions FWHM in mm (point source sensitivities in cps-MBq) for half-cone beam, fan-beam and parallel-beam collimators were 5.2 (85.6), 5.1 (55.6) and 5.9 (39.7), respectively. Image quality was evaluated using a three-dimensional Hoffman brain phantom and patient data. The deeper gray matter were more clearly visualized in the half-cone beam scans. **Conclusion:** Half-cone beam collimation provides higher sensitivity and offers the potential for improved brain imaging compared with parallel-beam and fan-beam collimation when used with a triple-camera SPECT system.

Key Words: SPECT; half-cone beam; brain imaging

J Nucl Med 1996; 37:498–502

Multiple-camera systems with parallel-hole collimators are widely used in SPECT to increase the photon detection efficiency (*1,2*). In brain imaging using large field of view cameras, the photon detection efficiency can be further increased by using converging fan-beam or cone-beam collimators (*3–11*). By magnifying both the axis of rotation direction and the direction perpendicular to the axis of rotation, cone-beam collimation provides the highest photon detection sensitivity among collimators having similar resolution characteristics.

Studies have shown that the use of cone-beam collimation increases the detectability of lesions, compared with parallel- and fan-beam collimation techniques (*12,13*). To optimize both resolution and field of view in brain imaging, the collimators need to be as close to the patient's head as possible. As demonstrated in Figure 1, however, this positioning has proven to be a problem when a conventional cone-beam (full-cone beam) collimator is used, because of the interference with patient's shoulders. Clearance of the shoulders by the cone-beam collimator results in truncation of the lower part of the brain during scanning. In SPECT imaging using a single camera, the truncation problem may be solved by tilting the collimator (*14,15*). When triple-camera SPECT systems are used, however, it is impossible to simultaneously tilt all three collimators while maintaining close proximity to the brain. In this study, a different approach has been used to clear the patient's shoulders. A half-cone beam (HCB) collimator has been designed and built for brain imaging (*16*). The focal point of the HCB collimator is located caudally towards the base of the brain to form a half-cone, as demonstrated in Figure 1. This geometry allows the HCB collimator to be close to the patient's head, thereby improving spatial resolution. We have compared the HCB collimator with commercially available parallel- and fan-beam collimators with similar resolution characteristics. Spatial resolutions (both planar and SPECT) and sensitivities of three collimators were measured, and image quality was evaluated using a three-dimensional Hoffman brain phantom and patient data. Please note that different radii of rotation were used in the measurements because the experiments were performed over a period of time. We believe that the slightly different radii of rotation, however, should not change the conclusion of this article.

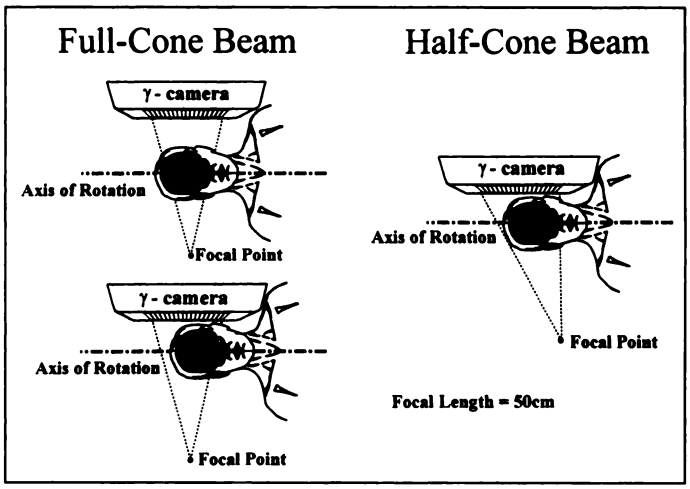

FIGURE 1. Schematic arrangement for brain imaging using half-cone beam and full-cone beam collimation. In the full-cone beam geometry, the clearance of the patient's shoulders may cause the lower part of the brain to be truncated. The focal length of both collimators is 50 cm.

MATERIALS AND METHODS

Collimators

The HCB collimator (Nuclear Fields, Inc., Des Plaines, IL) was manufactured using lead casting methodology and has hexagonally shaped holes and a focal length of 50 cm (measured from the front surface of the collimator). Commercially available low-energy, super-high resolution (LESR) parallel-beam (PB), and low-energy, super-high resolution fan-beam (LESR-FB) collimators were used for comparison studies. All collimators had a rectangular field of view of 45.6 × 22.8 cm at the crystal surface. Table 1 lists the specifications of the three collimators. The collimators were mounted on our triple-camera SPECT system (Trionix Research Laboratories, Twinsburg, OH), and simultaneous projections were acquired with all three collimators. Compensation for regional nonuniformities in the SPECT detector system was performed

Received Apr. 18, 1995; revision accepted Aug. 16, 1995.
For correspondence or reprints contact: Ronald J. Jaszczak, PhD, Department of Radiology, DUMC-3949, Duke University Medical Center, Durham, NC 27710.

TABLE 1
Collimator Specifications

Collimator	Hexagonal hole size (flat-to-flat) (mm)	Hole length (mm)	Septal thickness (mm)	Focal length (patient side) (mm)
LESR-PB	1.40	44.4	0.18	—
LESR-FB	1.22	41–46	0.15	380
HCB	1.45	40–52	0.22	500

extrinsically. The correction matrices were determined using the manufacturer's software based on high-count (100 million counts) flood phantom images acquired before all the measurements.

Resolution and Sensitivity

Planar system spatial resolutions (FWHM, and FWTM) and sensitivity were measured using small (approximately 1-mm diameter) in-air line and point sources, respectively. Planar system spatial resolutions (FWHM and FWTM) and sensitivity measurements were also obtained using the LESR-PB and LESR-FB collimators. Technetium-99m-pertechnetate was used in the measurements. Spatial resolution and sensitivity were measured for the HCB collimator as functions of distance from the collimator surface and compared with those of LESR-PB and LESR-FB collimators. Measurements were obtained with sources at 5, 10, 15 and 20 cm from the collimator surface. In measurements using the HCB collimator, sources were positioned 1 cm away from the midline to avoid truncation. The midline corresponds to an imaginary line perpendicular to the surface of the NaI(Tl) crystal that passes through the focal point.

SPECT spatial resolution (FWHM) was measured for each of the three collimators using an in-air ^{99m}Tc line source located on the axis of rotation 14 cm from the collimator surface. The SPECT acquisition matrix was 256 × 128 × 120 angular views over 360°. The linear sampling was 1.78 mm (for a point located on the detector surface) in both transaxial and axial directions. The radius of rotation was equal to 14 cm.

Volume sensitivities were measured for each of the three collimators using the three-dimensional Hoffman brain phantom (Data Spectrum Corp., Hillsborough, NC). The phantom was filled with uniformly distributed [^{99m}Tc]pertechnetate. The center of the cylinder was 12 cm from the collimator surface. Four sets of projections, equally spaced over 360°, were acquired. These projections were decay-corrected and were summed to minimize the count variations due to brain phantom asymmetry.

Hoffman Brain Phantom Imaging

The three-dimensional Hoffman brain phantom filled with [^{99m}Tc]pertechnetate (780 MBq) was used to evaluate half cone-beam SPECT image quality. Simultaneous projections of the brain phantom were acquired using all three collimators to ensure an equal scan time. The center-of-rotation calibrations for all collimators were carefully performed using a point source (*17*). The radius of rotation for the phantom scans was 11 cm measured from the front surface of the collimators. A primary energy window (130 keV ≤ Eγ ≤ 151 keV) and a scatter energy window (89 keV ≤ Eγ ≤ 127 keV) were used for the SPECT scans and corresponded to the 15% and 35% window widths, respectively. The SPECT acquisition matrix was 256 × 128 × 180 angular views over 360°. The linear sampling was 1.78 mm (for a point located on the detector surface) in both the transaxial and axial directions. Two scans, one short scan and one long, were acquired. The total acquisition times for the short and long scans were 30 min and 3 hr, respectively. Decay-correction was performed on projections in both scans.

Patient Imaging

Exametazine brain perfusion scans were performed on three patients (two women, one man) using the HCB collimator, as well as the LESR-PB and LESR-FB collimators. The amount of radioactivity ranged from 590 to 860 MBq (calibrated to the time when scans were started). The radii of rotation ranged from 13.0 to 13.5 cm. Only one energy window (primary window) was used in the patient scans. The SPECT acquisition matrix was 128 × 64 × 120 angular views over 360°. The linear sampling was 3.56 mm (for a point located on the detector surface) in both transaxial and axial directions. Total acquisition times ranged from 20 to 30 min.

Image Reconstruction

SPECT data were reconstructed using a filtered backprojection reconstruction algorithm. A three-dimensional cone-beam filtered backprojection algorithm (*18*) was modified for HCB SPECT reconstruction. In reconstructions with phantom data, the projections were first reduced from matrix size 256 × 128 to 128 × 64, and then precorrected for scatter using the projections obtained from the second energy window. The dual-window subtraction method was used (*19*). The scatter subtraction constant k (0.4) was used. The scatter subtract constant k was determined heuristically using a point source both in air and water (*19*). Attenuation compensation was performed for the phantom images because the location and size of the three-dimensional brain phantom were known. Attenuation compensation was not performed for the patient scans. The multiplicative Chang's attenuation correction method was used to compensate for the attenuation (*20*). A uniform attenuation map (attenuation coefficient $\mu = 0.153\ cm^{-1}$) was generated based on the phantom size and experimental setup. A reconstruction matrix size of 128 × 128 × 64 slices was used for all reconstructions. The matrix size corresponded to a 3.56-mm pixel size and slice thickness. In reconstructions using phantom data obtained with the 3-hr scan, band-limited ramp filters were used. In reconstructions using the patient data and the brain phantom data obtained with the 30-min scan, generalized Hann apodizing functions were used. The cutoff frequencies were chosen so that the reconstructed SPECT resolutions of the line source on the axis of rotation for all three collimators were equal.

RESULTS

Resolution and Sensitivity

The measured planar resolutions, FWHM and FWTM, as functions of distance from the collimator surface for the three collimators are shown in Figures 2 and 3, respectively. We define planar resolutions as the FWHM (FWTM) measured with a stationary (planar), single-view acquisition. The measured planar sensitivities are shown in Figure 4. All three collimators had similar resolution characteristics. As demonstrated in Figure 4, however, the HCB collimator provided much higher sensitivity compared with the LESR-PB and LESR-FB collimators. At 10-cm from the collimator surface, the sensitivities measured using a ^{99m}Tc point source for the half-cone, fan- and parallel-beam collimators were 85.6, 55.6 and 39.7 cts/(sec-MBq), respectively.

Reconstructed SPECT resolutions (using ramp filters) at 14 cm from the collimators were 6.6 mm, 6.0 mm and 7.0 mm for the HCB, LESR-FB and LESR-PB collimators, respectively. These SPECT resolutions were very close to the corresponding planar resolutions.

Volume sensitivities for all three collimators were measured using the three-dimensional Hoffman brain phantom. With the center of the brain phantom placed at a distance of 12 cm from the collimator surface, the volume sensitivities for the half-cone, fan- and parallel-beam collimators were 28,836, 17,829 and 13,419 cts/(sec-MBq-ml), respectively.

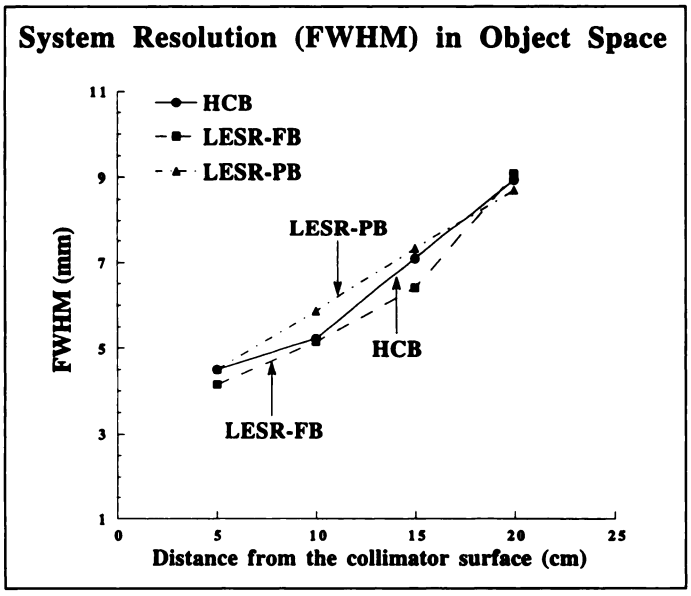

FIGURE 2. The measured planar resolution (FWHM) as a function of distance from the collimator surface for half-cone beam, low-energy, super-high resolution fan-beam and low-energy, super-high resolution, parallel-beam collimators.

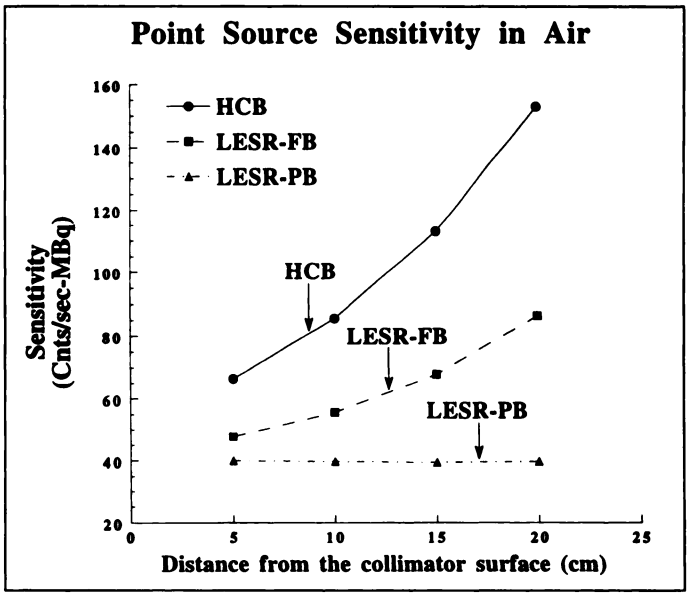

FIGURE 4. The measured planar sensitivities as a function of distance from the collimator surface for half-cone beam, low-energy, super-high resolution fan-beam and low-energy, super-high resolution, parallel-beam collimators. An in-air point source was used for the planar sensitivity measurements.

Hoffman Brain Phantom Imaging

The transverse sectional images and profiles of the high-count density scans of the three-dimensional Hoffman brain phantom using HCB, LESR-FB and LESR-PB collimators are shown in Figure 5. This slice was about 6 cm from the central plane of the HCB collimator. The same slice from the bitmap of the three-dimensional Hoffman brain phantom is also shown. Two reconstructed image slices (3.56 mm slice thickness) were added to match the slice thickness of the bitmap. The final slice thickness was 7.1 mm. As demonstrated in Figure 5, the HCB reconstructed image very closely resembled the bitmap. In the scans with high-count density and relatively low noise, the transverse sectional images obtained using the three collimators demonstrated similar contrast. Figure 6 shows the coronal sectional images of the same reconstructions. Two profiles are shown. One profile is through the superior portion of the parietal lobes, and the other is through the level of the temporal lobes of the Hoffman brain phantom. The profiles through the level of the temporal lobes demonstrate similar image contrast among three images. A slight

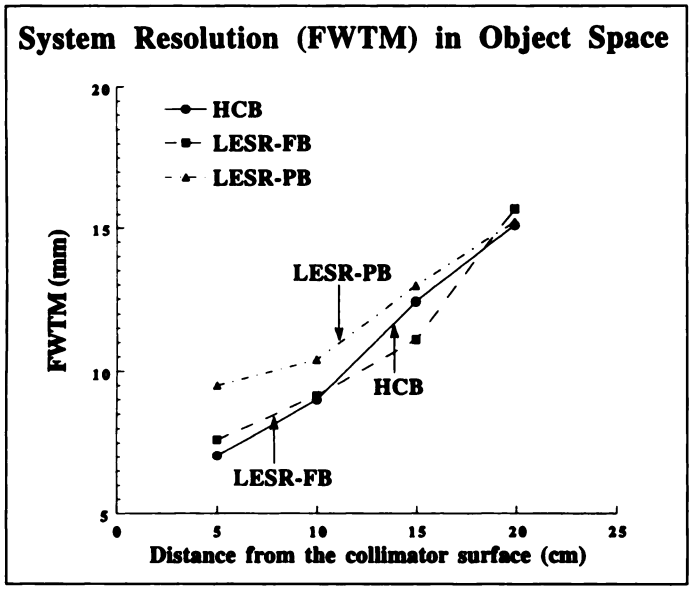

FIGURE 3. The measured planar resolution (FWTM) as a function of distance from the collimator surface for half-cone beam, low-energy, super-high resolution fan-beam and low-energy, super-high resolution parallel-beam collimators.

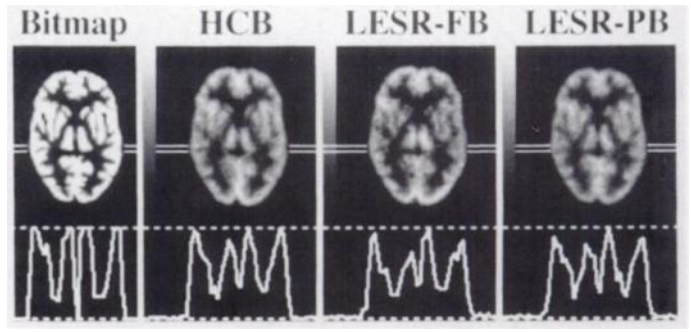

FIGURE 5. Transverse sectional images and profiles of the Hoffman brain phantom from a high-count density scan. Also shown is the corresponding slice of the bitmap of this phantom. This slice was about 6 cm from the central plane of the half-cone beam collimator.

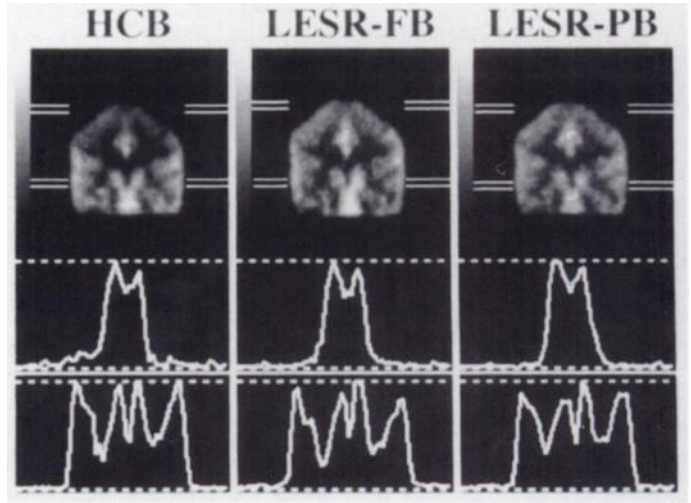

FIGURE 6. Coronal images and profiles of the Hoffman brain phantom from a high-count density scan. Two profiles are shown.

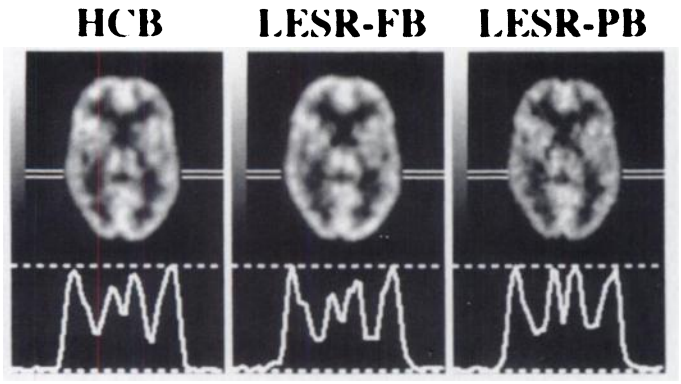

FIGURE 7. Transverse sectional images and profiles of the Hoffman brain phantom from a low-count density scan. This slice was about 6 cm from the central plane of the half-cone beam collimator.

distortion in count densities, however, can be seen in the most superior region in the HCB reconstruction.

The transverse sectional images and profiles of the low-count density scans of the three-dimensional Hoffman brain phantom using HCB, LESR-FB and LESR-PB collimators are shown in Figure 7. This slice was about 6 cm from the central plane of the HCB collimator, and the figure shows two-slice images 7.1-mm thick. In the scans with low-count density, the transverse sectional image obtained using the HCB collimator demonstrates improved noise characteristics compared with the images obtained using the LESR-FB and LESR-PB collimators.

Patient Imaging

Figures 8 and 9 show the transverse and sagittal sectional images and profiles of a patient scan, respectively. The images are two-slice images 7.1-mm thick and were not attenuation-corrected.

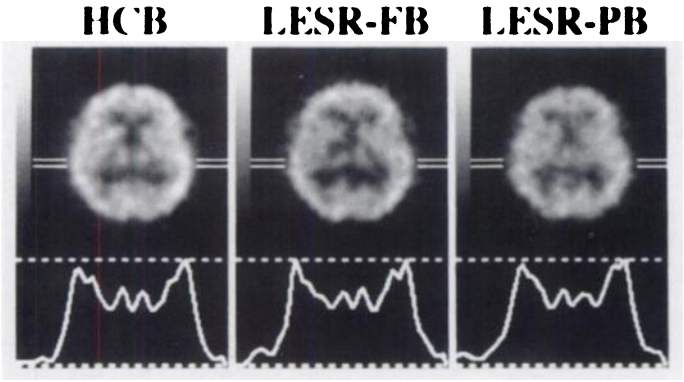

FIGURE 8. Transverse sectional images and profiles of a patient scan. The slice is 7.1-mm thick.

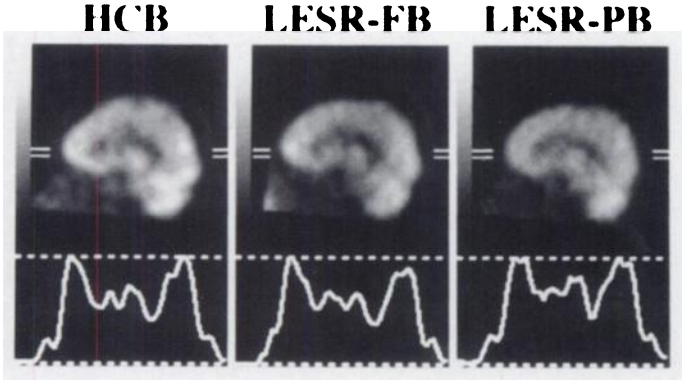

FIGURE 9. Sagittal images and profiles of a patient scan. The slice is 7.1-mm thick.

The images are noisier than the typical images, because projections for each of the images were acquired using only one head of the triple-camera SPECT system with the typical clinical scan parameters (activity concentration, scan time, etc.). The HCB images demonstrate improved image quality and better noise characteristics compared with LESR-FB and LESR-PB images. The deeper gray matter structures are more clearly visualized in the HCB scans. Much like the phantom images, however, a slight distortion in count densities was observed in the most superior region in the sagittal view of the HCB reconstruction.

DISCUSSION

A specially designed high-resolution, HCB collimator has been developed for brain imaging with triple-camera SPECT systems, for which tilting the cameras to clear the patient's shoulders is impossible. The focal point of the HCB collimator is located towards the base of the brain to form a half-cone. This geometry allows the HCB collimator to be close to the patient's head, thereby improving spatial resolution and increasing the useful field of view. We have compared the HCB collimator with parallel- and fan-beam collimators with similar resolution characteristics. For equivalent spatial resolution characteristics, the HCB collimator offers the potential for a 1.4 and 1.7 factor gain in volume sensitivity when compared with the commercially available super-high resolution fan-beam and parallel-beam collimators, respectively. It should be noted that the fan-beam collimator had a shorter focal length (38 cm) compared with the HCB collimator (50 cm). A HCB collimator with focal length of 50 cm was selected mainly to ensure an adequate axial field of view for imaging the brain, because the axial field of view of our current triple-camera system is only 22.8 cm. Larger axial field of view systems are available today. With newer triple-camera SPECT systems that have larger axial fields of view, the focal length of the HCB collimator could be decreased. Its sensitivity would then be further increased compared with the 50-cm HCB collimator used in this study.

Images obtained using the HCB collimator demonstrated improved overall image quality and noise characteristics. The deeper gray matter structures were visualized more clearly in the HCB scans. The results indicate that HCB collimation provides higher sensitivity and may offer the potential for improved brain imaging compared with parallel- and fan-beam collimators in conjunction with a triple-camera SPECT system.

With a single circular orbit, axial blurring and distortions are observed in HCB reconstructions for locations some distance from the midplane. The distortion is the result of inadequate sampling and the lack of appropriate filtering along the axis of rotation direction in HCB geometry. The HCB geometry places the top of the brain further from the central plane of the cone-beam geometry than does the full-cone beam geometry. This means that the axial blurring of the top of the brain for the HCB collimator is expected to be worse than that for a full-cone beam collimator, because the blurring artifacts become worse with distance from the central plane of the cone-beam geometry in the FBP reconstruction using a Feldkamp-type algorithm. We previously demonstrated that the maximum likelihood-expectation maximization algorithm provided less axial distortion than the FBP algorithm in full-cone beam and pinhole SPECT (*21,22*). Other investigations have demonstrated similar results for the full-cone beam collimation (*23*). We are currently investigating iterative reconstruction approaches for HCB geometry.

There are also several acquisition approaches that could be implemented to minimize axial blurring artifacts. One approach is to use longer focal length collimators. This approach, however, would decrease the gain in sensitivity. Astigmatic HCB collima-

tors with shorter in-plane focal length and longer axial focal length can minimize the inadequate axial sampling while maintaining a gain in sensitivity. With the use of astigmatic HCB collimators, the in-plane focal length can be shortened to obtain better tradeoff between resolution and sensitivity. With triple-camera SPECT systems, another solution is to combine HCB, fan-beam and parallel-beam collimators to obtain adequate axial sampling. Simultaneous acquisition can be performed with triple-camera systems by using two HCB collimators and a single parallel-beam or fan-beam collimator (*21*). The loss in overall sensitivity (relative to the use of three HCB collimators) is only about 15%–20%.

ACKNOWLEDGMENTS

This work was supported by Public Health Service grant R01-CA33541 awarded by the National Cancer Institute and by Department of Energy grant DE-FG02-96ER62150. We are grateful to Ms. Nancy Jaszczak (Data Spectrum Corp., Hillsborough, NC) for allowing us to use the three-dimensional Hoffman Brain phantom. One author (RJJ) is a consultant to, and an officer of, Data Spectrum Corp.

REFERENCES

1. Lim CB, Chang LT, Jaszczak RJ. Performance analysis of three camera configurations for SPECT. *IEEE Trans Nucl Sci* 1980;27:559–568.
2. Jaszczak RJ, Coleman RE, Lim CB. Single-photon emission computed tomography. *IEEE Trans Nucl Sci* 1980;27:1137–1153.
3. Jaszczak RJ, Chang LT, Murphy PH. SPECT using multi-slice fan-beam collimators. *IEEE Trans Nucl Sci* 1979;26:610–618.
4. Tsui BMW, Gullberg GT, Edgerton ER, Gilland DR, Perry JR, McCartney WH. Design and clinical utility of a fan-beam collimator for SPECT imaging of the head. *J Nucl Med* 1986;27:810–819.
5. Jaszczak RJ, Floyd CE, Manglos SH, Greer KL, Coleman RE. Cone-beam collimation for SPECT: analysis, simulation and image reconstruction using filtered backprojection. *Med Phys* 1986;13:484–489.
6. Jaszczak RJ, Greer KL, Coleman RE. SPECT using a specially designed cone-beam collimator. *J Nucl Med* 1988;29:1398–1405.
7. Hawman EG, Hsieh J. An astigmatic collimator for high sensitivity SPECT of the brain [Abstract]. *J Nucl Med* 1986;27(suppl):930.
8. Smith BD. Cone beam tomography: recent advances and tutorial review *Opt Eng* 1990;29:524–534.
9. Zeng GL, Tung CH, Gullberg GT. New approaches to reconstructing truncated projections in cardiac fan beam and cone beam tomography [Abstract]. *J Nucl Med* 1990;31(suppl): 867.
10. Gullberg GT, Zeng GL, Christian PE, Datz FL, Morgan HT. Cone-beam tomography of the heart using SPECT. *Invest Radiol* 1991;26:681–688.
11. Gullberg GT, Zeng GL, Datz FL, Christian PE, Tung CH, Morgan HT. Review of convergent beam tomography in SPECT. *Phys Med Biol* 1992;37:507–534.
12. Tsui BMW, Terry JA, Gullberg GT. Evaluation of cardiac cone-beam SPECT using observer performance experiments and receiver operating characteristic analysis. *Invest Radiol* 1993;28:1101–1112.
13. Li J, Jaszczak RJ, Turkington TG, Metz CE, Gilland DR, Greer KL, Coleman RE. An evaluation of lesion detectability with cone-beam, fan-beam and parallel-beam collimation in SPECT by continuous ROC study. *J Nucl Med* 1994;35:135–140.
14. Jaszczak RJ, Greer KL, Floyd CE, Manglos SH, Coleman RE. Imaging characteristics of a high-resolution cone-beam collimator *IEEE Trans Nucl Sci* 1988;35:644–648.
15. Manglos SH, Jaszczak RJ, Greer KL. Cone-beam SPECT reconstruction with camera tilt. *Phys Med Biol* 1989;34:625–631.
16. Jaszczak RJ, Li J, Wang H, Jang S, Coleman RE. Half-cone beam collimation for triple-camera SPECT system. *Eur J Nucl Med* 1994;21:S9.
17. Li J, Jaszczak RJ, Wang H, Greer KL, Coleman RE. Determination of both mechanical and electronic shifts in cone-beam SPECT. *Phys Med Biol* 1993;38:743–754.
18. Feldkamp LA, Davis LC and Kress JW. Practical cone-beam algorithm. *J Opt Soc Am* 1984;A1:612–619.
19. Jaszczak RJ, Greer KL, Floyd CE, Harris CC, Coleman RE. Improved SPECT quantification using compensation for scattered photons. *J Nucl Med* 1984;25:893–900.
20. Chang LT. A method for attenuation correction in radionuclide computed tomography. *IEEE Trans Nucl Sci* 1978;25:638–643.
21. Jaszczak RJ, Li J, Wang H, Greer KL, Coleman RE. Three-dimensional SPECT reconstruction of combined cone-beam and parallel-beam data. *Phys Med Biol* 1992;37:535–561.
22. Jaszczak RJ, Li J, Wang H, Zalutsky MR, Coleman RE. Pinhole collimation for ultra-high resolution, small field of view SPECT. *Phys Med Biol* 1994;39:425–437.
23. Zeng GL, Gullberg GT. A study of reconstruction artifacts in cone-beam tomography using filtered backprojection and iterative EM algorithms. *IEEE Trans Nucl Sci* 1990;37:759–767.

Effects of Hypoxia on the Uptake of Tritiated Thymidine, L-Leucine, L-Methionine and FDG in Cultured Cancer Cells

Anaira C. Clavo and Richard L. Wahl

Division of Nuclear Medicine, Department of Internal Medicine, University of Michigan, Ann Arbor, Michigan

We previously demonstrated in vitro that FDG uptake into viable cancer cells increases in the presence of hypoxic versus normoxic conditions. Since positron-emitter labeled thymidine and amino acids are being used for PET, we evaluated uptake into tumor cells of several tracers (thymidine, L-leucine, L-methionine and FDG) in the presence of either normoxic or hypoxic atmospheres in vitro. **Methods:** Uptake of tritiated thymidine, L-leucine, L-methionine and FDG into two human tumor cell lines (HTB 63 melanoma and HTB 77 IP3 ovarian carcinoma) was determined after a 4-hr exposure to each of three different oxygen atmospheres (0, 1.5 and 20% O_2) in vitro. **Results:** Under moderately hypoxic conditions (1.5% O_2), thymidine uptake decreased significantly from the 20% O_2 baseline for both melanoma and ovarian carcinoma cell lines (33% and 15%, respectively) and with anoxia, thymidine uptake declined from baseline by 43% and 21%, respectively. Leucine uptake decreased substantially in the melanoma cells, by 23% when exposed to 1.5% O_2 and 36% in the presence of 0% O_2, but only modestly or not at all in the IP3 cells. After 1.5% or 0% O_2 exposure, methionine uptake was not significantly different from 20% O_2 levels in either cell line. In contrast, FDG uptake in both cell lines increased significantly (23% and 38%, respectively) over normoxic (20% O_2) conditions when cells were exposed to moderate hypoxia. FDG uptake also increased over basal conditions after anoxia, by 11% and 30% for melanoma and ovarian carcinoma cells, respectively. **Conclusion:** Hypoxia decreases cellular uptake of thymidine and increases FDG uptake in two different malignant human cell lines. Leucine uptake decreases with hypoxia in the melanoma cell line but not markedly in the IP3 cell line, while hypoxia does not alter methionine uptake in either cell line significantly. Hypoxia has varying effects on metabolic tracers used for PET. The use of paired hypoxia-sensitive PET tracers has potential for noninvasively characterizing tissue oxygenation levels.

Key Words: fluorine-18-fluorodeoxyglucose; hypoxia; nucleotide uptake; amino acid uptake

J Nucl Med 1996; 37:502–506

Received Apr. 13, 1995; revision accepted Aug. 17, 1995.

For correspondence or reprints contact: Richard L. Wahl, MD, Division of Nuclear Medicine, University of Michigan Medical Center, 1500 E. Medical Center Dr., B1G 412, Ann Arbor, MI 48109-0028.